Low Temperature Physics/Fizika Nizkikh Temperatur, 2012, v. 38, No. 6, pp. 644–652

Conductance of a STM contact on the surface of a thin film

N.V. Khotkevych and Yu.A. Kolesnichenko

B. Verkin Institute for Low Temperature Physics and Engineering of the National Academy of Sciences of Ukraine
47 Lenin Ave., Kharkov 61103, Ukraine
E-mail: khotkevych@ilt.kharkov.ua

J.M. van Ruitenbeek

Kamerlingh Onnes Laboratorium, Universiteit Leiden, Postbus 9504, 2300 Leiden, The Netherlands

Received January 12, 2012

The conductance of a contact, having a radius smaller than the Fermi wave length, on the surface of a thin metal film is investigated theoretically. It is shown that quantization of the electron energy spectrum in the film leads to a step-like dependence of differential conductance $G(V)$ as a function of applied bias eV. The distance between neighboring steps in eV equals the energy level spacing due to size quantization. We demonstrate that a study of $G(V)$ for both signs of the voltage maps the spectrum of energy levels above and below Fermi surface in scanning tunneling experiments.

PACS: **74.55.+v** Tunneling phenomena: single particle tunneling and STM;
85.30.Hi Surface barrier, boundary, and point-contact devices;
73.50.–h Electronic transport phenomena in thin films.

Keywords: STM, surface barrier, thin film, conductance.

1. Introduction

Today a fairly large number of papers have addressed the problem of calculating point-contact conductance for use in analyzing and interpreting scanning tunneling microscopy (STM) experiments (for reviews see, for example, [1,2]). The low symmetry of the problem and the wide variety of objects under study do not allow developing a general theory of STM, and different approaches for specific problems are used. The theory papers on this subject can be divided into two groups: One uses methods taking into account the specific atomic structure of the STM tip and that of the test specimen. These methods make it possible to reproduce the crystallographic structure of the sample surface in the calculated STM images and this is very useful for arriving at a correct interpretation of experimental data. The main deficiency of this approach is the lack of analytical formulas for the STM current–voltage characteristics as numerical calculations must be performed for every specific case. The other group of works exploit simplified models of noninteracting electrons which allows finding relatively simple analytical expressions that describe the STM current qualitatively. For this reason such theoretical results are widely used by experimentalists.

One of the first free-electron models describing STM experiments was proposed by Tersoff and Hamann [3] whose theoretical analysis of tunnel current is based on Bardeen's formalism [4], in which a tunneling matrix element is expressed by means of independent wave functions for the tip and the sample within the barrier region. Using the model wave functions the authors [3] showed that the conductance of the system is proportional to the local density of states of the sample at the tip position. In principle it is possible to extract information on subsurface objects (single defects, clusters, interfaces, etc.) by STM, but this requires a more detailed theoretical analysis [5], which takes into account the influence of subsurface electron scattering on the tunneling current.

The physical picture of an electron tunneling through a classically forbidden region is that the electron flow emerging from the barrier is defined by the matching of the wave functions of carriers incident on the barrier and those that are transmitted. For a three-dimensional STM geometry the wave functions for electrons transmitted through the vacuum region radically differs from the electron wave functions in an isolated sample and they describe the electron propagation into the bulk from a small region on the surface below the STM tip. In contrast, the theory of Ref. 3 and its modifications (see [1,2] and references therein) uses unperturbed wave functions of the surface Bloch states. Changes in the wave functions of transmitted electrons due to scattering by subsurface objects provide the information about such scattering in the STM conductance.

In Ref. 6 it was proposed to introduce in the theory of STM the model by Kulik *et al*. [7]. In this model a three-dimensional STM tip is replaced by an inhomogeneous barrier in an otherwise nonconducting interface that separates the two conductors. In Ref. 7 it was shown that under assumption of small transparency of the tunnel barrier the wave function (and thus the current–voltage characteristics) can be found analytically for an arbitrary size of the tunnel area. The results in [6] for the conductance of the tunnel point contact were generalized to an arbitrary Fermi surface for the charge carriers in Refs. 8, 9. In a series of papers the model [7] has been expanded to describe oscillations of the STM conductance resulting from electron scattering by subsurface defects [6,8–11] (for reviews see [12]).

Scanning tunneling microscopes have been widely used for the study of various small-sized objects: islands, thin films deposited on bulk substrates, etc. [13–20]. First, a discrete periodic spatial variation of the STM current originating from the quantization of electron states was observed in the quantum wedge: a nanoscale flat-top Pb island on a stepped Si(111) surface [13]. Later these authors showed that the lattice structure of an interface buried under a film of Pb, whose thickness can be as many as 10 times the Fermi wavelength, can be clearly imaged with STM [14]. They concluded that the key to the transparency of a metal lies in a highly anisotropic motion of the electrons and the strong quantization of their transverse wave function components. In the paper [15] the electronic states of thin Ag films grown on GaAs(110) surfaces was investigated by STM with single-layer thickness resolution, and the quantum-well states arising from the confinement geometry of the Ag films have been identified. Quantum size effects, manifested in the formation of new electronic bound states, were investigated by STM on thin Pb islands of varying heights on the Si(111)-(7×7) surface in Ref. 16. In experiments [17] it was demonstrated that scanning tunneling microscopy and spectroscopy of epitaxial Pb islands on Si(111) reveal adiabatic lateral modulation of the energy spectra of the quantum well, providing remote electronic images of the subsurface reflection phase. In Ref. 18 a step structure at the buried Pb on Si(111) 6×6-Au interface was determined by utilizing the presence of quantum well states. It was demonstrated that the spatial step positions as well as the step heights can be extracted nondestructively and with atomic layer precision by STM. Vertical Friedel oscillations in interface-induced surface charge modulations of Pb islands of a few atomic layers on the incommensurate Si(111)–Pb surface have been observed [19]. Thus, detailed experimental results have been obtained, but a microscopic theory for STM tunneling spectra on samples of finite size has not been reported, which provides the motivation for the present work. Current–voltage characteristics for size quantization in planar thin film geometries of metal–insulator–metal tunneling junctions have been investigated theoretically in Refs. 21, 22. Standing electron wave states in thin Pb films have been observed by electron tunneling in early experiments by Lutskii *et al*. [23].

In this paper we present the differential conductance $G(V)$ for small contacts, having a radius a smaller than the Fermi wave length $\lambda_F = \hbar / p_F$, where p_F is the Fermi momentum. The contacts are formed on the surface of a thin metal film and we analyze the voltage dependence of $I(V)$ and $G(V)$. We focus on the size quantization effects of the electron energy spectrum in the film on $G(V)$.

The organization of this paper is as follows. The model that we use to describe the contact, and the method for obtaining a solution of the three-dimensional Schrödinger equation asymptotic in the small radius of the contact, are described in Sec. 2. In Sec. 3 the current–voltage characteristics and the differential conductance are found on the basis of a calculation of the probability current density through the contact. Section 4 presents a physical interpretation of the results obtained. In Sec. 5 we conclude by discussing the possibilities for exploiting these theoretical results for interpretation of electron energy spectroscopy in thin films by STM. In the Appendixes we solve the Schrödinger equation for the tunnel point contact in framework of our model (Appendix 1) and for a point contact without barrier (Appendix 2) and find the wave functions for electrons transmitted through the contact. These solutions are used in Sec. 3 for the calculation of current.

2. Model and electron wave function of the system

The model that we consider is illustrated in Fig. 1. Electrons can tunnel through an orifice centered at the point $\mathbf{r} = 0$ in an infinitely thin insulating interface at $z = 0$ from a conducting half-space (the tip) into a conducting sheet of thickness d (Fig. 1,*b*). The radius a of the contact and the thickness d of the film are assumed to be much smaller than the shortest mean free path, i.e., we consider a purely ballistic problem. The wave function ψ satisfies the Schrödinger equation

$$\nabla^2\psi(\mathbf{r}) + \frac{2m^*}{\hbar^2}\left[\varepsilon - U(\mathbf{r})\right]\psi(\mathbf{r}) = 0. \qquad (1)$$

In Eq. (1) m^* and ε are electron effective mass and energy, respectively. The inhomogeneous potential barrier in the plane $z = 0$ we describe by the function $U(\mathbf{r}) = U_0 f(\boldsymbol{\rho})\delta(z)$, where $\boldsymbol{\rho} = (x, y)$ is a two-dimensional position vector in the plane and $f^{-1}(\boldsymbol{\rho}) = \Theta(a - \rho)$, with $\Theta(x)$ the Heaviside step function. For such model the wave function $\psi(\mathbf{r})$ satisfies the following boundary conditions at the interface $z = 0$ and at the metal sheet surface $z = d$

$$\psi(\boldsymbol{\rho}, +0) = \psi(\boldsymbol{\rho}, -0), \qquad (2)$$

$$\psi'_z(\boldsymbol{\rho}, +0) - \psi'_z(\boldsymbol{\rho}, -0) = \frac{2m^*U_0}{\hbar^2} f(\boldsymbol{\rho})\psi(\boldsymbol{\rho}, 0), \qquad (3)$$

$$\psi(\boldsymbol{\rho}, d) = 0. \qquad (4)$$

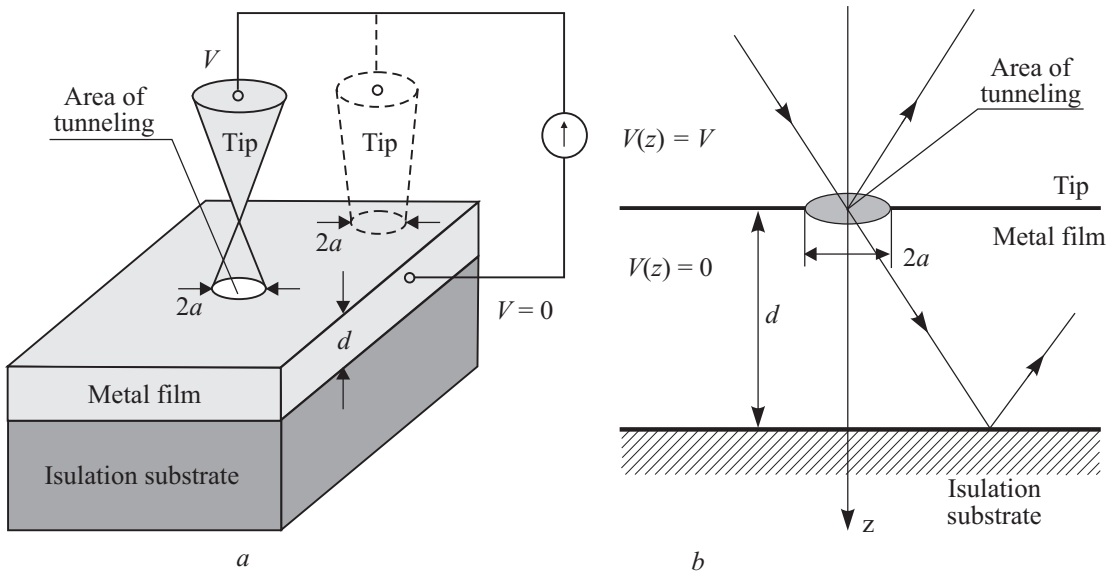

Fig. 1. Schematic representation of a STM experiment on a thin metal film (*a*) and the model that we employ to represent the contact between a bulk conductor (tip) and a metallic film (*b*). The dashed picture of the tip in *a* illustrates a metallic point contact (STM tip touches the surface). Electron trajectories in *b* are shown schematically.

Equations (1)–(4) can be solved in the limit of a small contact, $ka \ll 1$ ($k = \sqrt{2m^*\varepsilon}/\hbar$ is the absolute value of the electron wave vector $\mathbf{k}$). In the zeroth approximation in the contact diameter the solutions of Eq. (1) for $z \gtrless 0$ are independent and satisfy the zero boundary condition $\psi(\boldsymbol{\rho}, 0) = 0$ at the impenetrable interface at $z = 0$. The quantum states in the conducting half-space ($z < 0$) (the tip) are defined by the three components of the electron wave vector $\mathbf{k} = (\mathbf{k}_{\|}, k_z)$, with $\mathbf{k}_{\|}$ a two-dimensional vector parallel to the interface. In the metal film ($0 < z < d$) the quantum states are characterized by a two-dimensional vector κ perpendicular to the z axis and by the discrete quantum number n ($n = 1, 2, ...$) which results from the finite size of the conductor in the z direction. The energy eigenvalues and eigenfunctions for the two disconnected conductors are given by

$$\varepsilon = \frac{\hbar^2(k_{\|}^2 + k_z^2)}{2m^*} \equiv \frac{\hbar^2 k^2}{2m^*}, \tag{5}$$

$$\psi_0(\mathbf{r}) = 2ie^{i\mathbf{k}_{\|}\boldsymbol{\rho}} \sin k_z z, \qquad z < 0, \tag{6}$$

and

$$\varepsilon = \frac{\hbar^2(\kappa^2 + k_{zn}^2)}{2m^*}, \quad n = 1, 2, ..., \tag{7}$$

$$\psi_0(\mathbf{r}) = -2ie^{i\boldsymbol{\kappa}\boldsymbol{\rho}} \sin k_{zn} z, \qquad 0 < z < d, \tag{8}$$

where $k_{zn} = \pi n / d$. In Eqs. (6) and (8) we use a wave function normalization with unit amplitude of the wave incident to the interface.

The partial wave for the first order approximation $\psi_1(\mathbf{r})$ in the small parameter $ka \ll 1$, which describes the transition of electrons from one to the other conductor, is given in the Appendixes. Appendix 1, Eqs. (A1.5) and (A1.6), gives the solution for a tunnel point contact, having a potential barrier of small transparency $t = k\hbar^2 / m^* U_0 \ll 1$ at the orifice in the plane $z = 0$. Appendix 2, Eqs. (A2.6)–(A2.8), gives the solutions for a contact without barrier. Figure 2 illustrates the spacial variation of the square modulus of the wave function for electrons transmitted through the contact into the film.

3. Current–voltage characteristic and conductance of a point contact

As has been shown in Ref. 24 for a ballistic point contact of small radius a, with a much smaller than the electron mean free path l, the electrical potential $V(\mathbf{r})$ drops over a

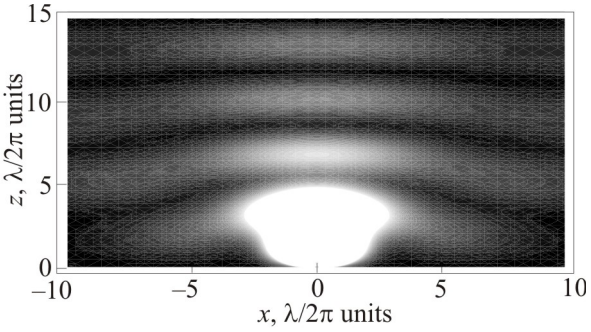

Fig. 2. Space distribution of the square modulus of the wave function for electrons injected by a STM tip into a metal sheet of thickness $d = 15$, where $\lambda = 2\pi / k$ is the electron wave length, $\lambda\!\!\!^{-} = \lambda / 2\pi$.

distance $r \sim a$ from the contact, and in the limit $a \to 0$ the potential $V(\mathbf{r})$ can be approximated by a step function $V\,\Theta(-z)$. In this approximation, for the calculation of the electrical current we can take the electron distribution functions $f^{(\mp)}$ at $z \lessgtr 0$ as the Fermi functions f_F with energies shifted by the applied bias eV (e is the negative electron charge), $f^{(\mp)} = f_F(\varepsilon - eV\Theta(-z))$. Figure 3 illustrates the occupied energy states in the two conductors for both signs of the applied bias eV. At $eV > 0$ the electrons flow from the bulk conductor (the tip) into the film and, vice-versa, at $eV < 0$ they flow from the film into the massive conductor. The total current through the area of the contact can be found by integration over the flux $J^{(\pm)}$ in both directions

$$I(V) = \frac{1}{2\pi d}\int\limits_{-\infty}^{\infty} d\boldsymbol{\kappa}\sum_{n=1}^{\infty} J^{(-)} f_F(\varepsilon)(1 - f_F(\varepsilon - eV)) -$$

$$- \frac{2}{(2\pi)^3}\int\limits_{-\infty}^{\infty} d\mathbf{k} J^{(+)} f_F(\varepsilon - eV)(1 - f_F(\varepsilon)). \qquad (9)$$

In Eq. (9) we integrate over the wave vector $\mathbf{k}$ in the semi-infinite conductor for the current in the negative direction (second term), and integrate over the two-dimensional wave vector κ and sum over the discrete quantum number n for the opposite direction of the current (first term).

For simplicity we will take the temperature to be zero. In this case the electric current is defined by electrons passing the contact in one direction only, depending on the sign of the applied bias. The flux $J^{(\pm)}$ integrated over the area of the contact is calculated in the usual way

$$J^{(\pm)} = \frac{|e|\hbar}{m^*}\int\limits_0^a d\rho\rho \int\limits_0^{2\pi} d\varphi\, \mathrm{Im}\left[\psi_1^*(\boldsymbol{\rho}, z)\frac{\partial}{\partial z}\psi_1(\boldsymbol{\rho}, z)\right]_{z=\pm 0}, \qquad (10)$$

where $\boldsymbol{\rho} = (\rho\cos\varphi, \rho\sin\varphi)$. The wave function $\psi_1(\boldsymbol{\rho}, z)$ should be taken as the wave transmitted through the contact, given by Eqs. (A1.5) and (A2.6) with $\mathbb{k} = k_z$ for electron flux from the tip to the sheet, $J^{(+)}$, and by Eqs. (A1.6) and (A2.7) with $\mathbb{k} = k_{zn}$ $(n = 1, 2\ldots)$ for fluxes $J^{(-)}$ in the opposite direction. The energy shift eV in the region $z < 0$ should be taken into account, which for our choice of the reference point of energy (see Fig. 3) implies that the absolute value of the electron wave vector in the half-space $z < 0$ is given by $\tilde{k} = \sqrt{2m^*(\varepsilon - eV)}/\hbar$.

For the tunnel point contact (tpc) the flux can be expressed in terms of the wave function in the contact plane (A1.1), and we obtain

$$J_{tpc}^{(+)} \simeq \frac{\pi^4 |e| a^4 \hbar^5 \tilde{k}^2 \cos^2\vartheta}{12 m^{*3} d^3 U_0^2} N(N+1)(2N+1), \qquad (11)$$

and

$$J_{tpc}^{(-)} \simeq -\frac{\pi |e| a^4 \hbar^5 \tilde{k}^3 k_{zn}^2}{6 m^{*3} U_0^2}. \qquad (12)$$

Here ϑ is the angle between the vector $\mathbf{k}$ and the z axis, and $N(k) = [kd/\pi]$ with $[x]$ the integer part of x.

For a metallic point contact (mpc) without barrier the expressions for the flux $J_{mpc}^{(\pm)}$ are written by means of Eqs. (A2.4), (A2.9)–(A2.11),

$$J_{mpc}^{(+)} \simeq \frac{\pi^2 |e| \hbar a^6 \tilde{k}^2 \cos^2\vartheta}{9 m^* d^3} N(N+1)(2N+1), \qquad (13)$$

and

$$J_{mpc}^{(-)} \simeq -\frac{8\pi |e| \hbar a^6 \tilde{k}^3 k_{zn}^2}{9 m^*}. \qquad (14)$$

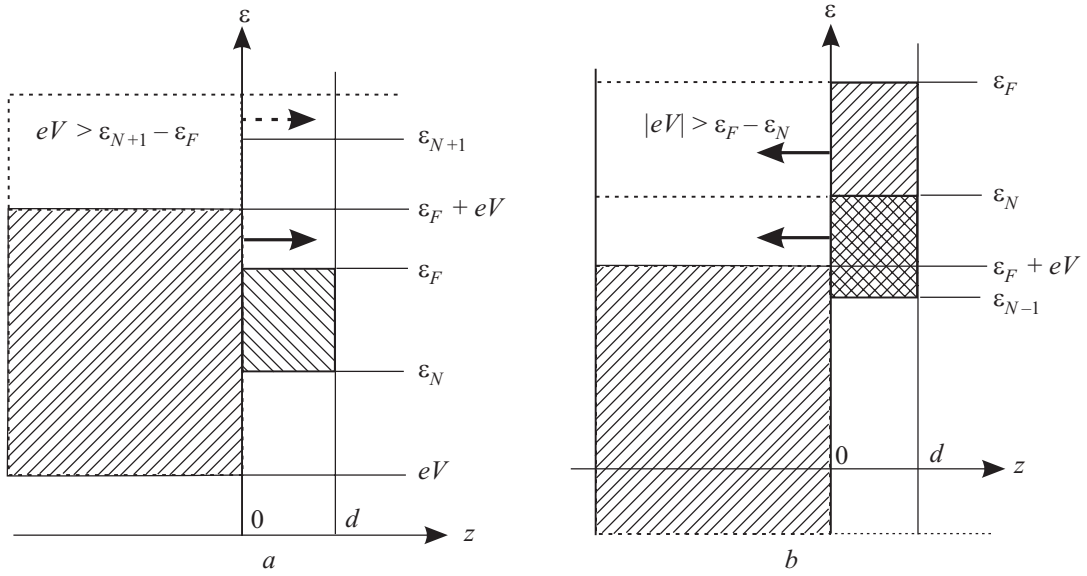

Fig. 3. Illustration of the occupied energy states at zero temperature in the two conductors for both signs of the applied bias eV: $eV > 0$ (*a*), $eV < 0$ (*b*).

Substituting Eqs. (11)–(14) into the general expression (9) we find the current–voltage characteristic of the system

$$I(V)=\frac{I_0}{(k_Fd)^3}\int\limits_{k_F}^{\tilde{k}_F}\frac{dkk^2}{k_F^5}(k^2-\frac{2meV}{\hbar^2})S_2(k),\quad eV\geqslant 0 \tag{15}$$

and

$$I(V)=-\frac{I_0}{(k_Fd)^3}\left\{S_2(k_F)\left[\frac{1}{5}+\frac{2}{3}\frac{|eV|}{\varepsilon_F}+\frac{1}{3}\left(\frac{|eV|}{\varepsilon_F}\right)^2\right]+\right.$$

$$+\left[S_3(\tilde{k}_F)-S_3(k_F)\right]\frac{\pi}{k_Fd}\left(\frac{|eV|}{\varepsilon_F}\right)^2+\frac{2}{3}\left[S_5(\tilde{k}_F)-S_5(k_F)\right]\times$$

$$\times\left(\frac{\pi}{k_Fd}\right)^3\frac{|eV|}{\varepsilon_F}+\frac{1}{5}\left[S_7(\tilde{k}_F)-S_7(k_F)\right]\left(\frac{\pi}{k_Fd}\right)^5-$$

$$\left.-S_2(\tilde{k}_F)\frac{\tilde{k}_F}{5k_F}\left[1+\frac{4}{3}\frac{|eV|}{\varepsilon_F}-\frac{8}{3}\left(\frac{|eV|}{\varepsilon_F}\right)^2\right],\quad eV\leqslant 0,\right. \tag{16}$$

where $\varepsilon_F=\hbar^2k_F^2/2m^*$ is the Fermi energy,

$$I_{0,tpc}=\frac{|e|\pi^2a^4\hbar^5k_F^8}{12m^{*3}U_0^2}, \tag{17}$$

$$I_{0,mpc}=\frac{e\hbar a^6k_F^8}{9m^*}, \tag{18}$$

$S_m(k)$ is a finite sum of mth powers of integer numbers

$$S_m(k)=\sum_{n=1}^{N(k)}n^m. \tag{19}$$

Note that $S_m(k)\equiv H_{-m}(N)$, where $H_m(n)$ are generalized harmonic numbers. The current is plotted in Fig. 4 as a function of bias voltage for two choices of the film thickness. Differentiating Eqs. (15) and (16) with respect to voltage we obtain the differential conductance $G(V)=dI/dV$ for a point contact with radius $a\ll\lambda_F$,

$$G(V)=G_1\left\{\frac{\tilde{k}_F}{2k_F}S_2(\tilde{k}_F)-\frac{1}{k_F^3}\int\limits_{k_F}^{\tilde{k}_F}dkk^2S_2(k)\right\},\quad eV\geqslant 0; \tag{20}$$

$$G(V)=G_1\left\{\frac{4}{3}\left[1+\frac{|eV|}{\varepsilon_F}\right]S_2(k_F)+4\frac{|eV|}{\varepsilon_F}\frac{\pi}{k_Fd}\left[S_3(\tilde{k}_F)-S_3(k_F)\right]+\right.$$

$$+\frac{4}{3}\left(\frac{\pi}{k_Fd}\right)^3\left[S_5(\tilde{k}_F)-S_5(k_F)\right]-$$

$$\left.-\frac{k_F}{3\tilde{k}_F}\left[1+4\frac{|eV|}{\varepsilon_F}-8\left(\frac{|eV|}{\varepsilon_F}\right)^2\right]S_2(\tilde{k}_F)\right\},\quad eV\leqslant 0. \tag{21}$$

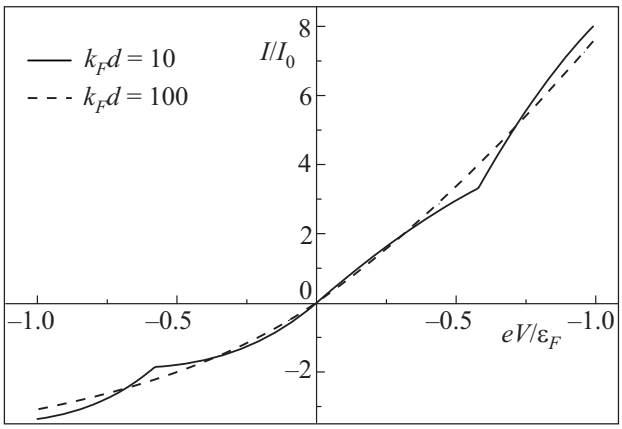

Fig. 4. Dependence of the total current, $I(V)$, on the applied bias over the point contact for two choices of the thicknesses of the metal film. The constant I_0 is given by Eq. (17) or Eq. (18).

In the limit $eV\to 0$ the zero-bias conductance taken from both sides coincides, as it should,

$$G(0)=G_1S_2(k_F)=\frac{G_1}{6}N_F(N_F+1)(2N_F+1), \tag{22}$$

where $N_F=N(k_F)$, and G_1 is the conductance of the contact between the bulk conductor (the tip) and a thin film that has only a single energy level available below ε_F for the motion along z,

$$G_1=G_0(0)\frac{3\pi^3}{(k_Fd)^3}. \tag{23}$$

$G_0(0)$ is the conductance of a contact between two conducting unbound half-spaces. For a tunnel point contact this is given by [7,12]

$$G_{0,tpc}(0)=\left(\frac{k_F\hbar^2}{m^*U_0}\right)^2\frac{e^2(k_Fa)^4}{36\pi\hbar}, \tag{24}$$

and for a metallic point contact we have [25]

$$G_{0,mpc}(0)=\frac{8e^2(k_Fa)^6}{27\pi^3\hbar}. \tag{25}$$

For $d\to\infty$ Eqs. (20) and (21) transform into the known voltage dependence of the conductance for a point contact between unbound conducting half-spaces [27],

$$G_0(V)=G_0(0)\left[1+\frac{|eV|}{\varepsilon_F}-\frac{1}{3}\left(\frac{|eV|}{\varepsilon_F}\right)^3\right]. \tag{26}$$

The dependence of the differential conductance $G(V)$ for both signs of applied voltage is illustrated in Fig. 5. For comparison the dependence $G_0(V)/G_0(0)$ from Eq. (26) is also shown.

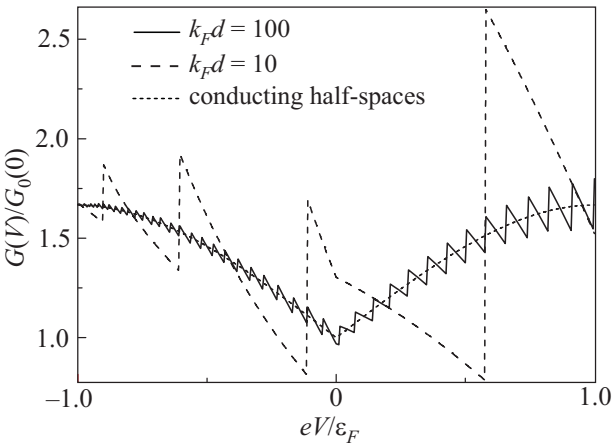

Fig. 5. Dependence of the normalized differential conductance, $G(V)/G_0(0)$, on the applied bias over the point contact for two choices of the thicknesses of the metal film. The voltage dependence for a point contact between two semi-infinite bulk conductors is shown for comparison (short-dashed curve).

4. Discussion

Thus, in the framework of the model illustrated in Fig. 1 we have obtained the current–voltage characteristic and the differential conductance for a contact on the surface of a thin metal film. Under the assumption that the contact radius a is much smaller than the Fermi wave length λ_F we found asymptotically exact formulas for the dependence of the total current $I(V)$ (Eqs. (15) and (16)) and the contact conductance $G(V)$ (Eqs. (20), (21)) on the applied voltage. In the limit of zero temperature and neglecting scattering processes we have demonstrated that the $I(V)$ dependence has kinks and $G(V)$ undergoes jumps at the same values of applied bias eV (see Figs. 4 and 5). These events result from the size quantization of the electron spectrum in the film.

The results obtained show that even in Ohm's-law approximation (22), $eV \to 0$, the conductance $G(V)$ is not simply proportional to the electron density of states (DOS) in the isolated film,

$$\rho_f(\varepsilon) = \frac{m^* N_F}{\pi\hbar^2 d}. \qquad (27)$$

It is remarkable that the dependence of the conductance $G(0)$ (22) on the number of quantum levels N_F is the same for, both, tunnel and metallic point contacts. This fact shows that such dependence is not sensitive to the model taken for the potential barrier, and that it is the result of the point-contact geometry. Recently, the relationship between the differential conductance and the local density of states has been studied in a tight-binding approximation for tunnel junctions, where the junction geometry can be varied between the limiting cases of a point-contact and a planar junction [28]. In the framework of a real-space Keldysh formalism the authors of Ref. 28 have shown that the differential conductance is not, in general, proportional to the sample DOS for planar junctions, although features of the DOS may be present.

From Eqs. (20) and (21) it follows that the conductance is nonsymmetric in the applied bias. This asymmetry can be explained as follows: Let $eV > 0$ and electrons tunnel from the bulk conductor into the film (Fig. 3,*a*) in which N_F subbands of the size quantization are partially filled. If the bias eV is smaller than the distance $\Delta\varepsilon$ between the Fermi level ε_F and the bottom of the next (empty) subband $\varepsilon_{N+1} = \pi^2\hbar^2(N_F+1)^2/2m^*d^2$, $\Delta\varepsilon = \varepsilon_{N+1} - \varepsilon_F$, the electron can tunnel into any of the N_F subbands. At $eV = \Delta\varepsilon$ tunneling into the (N_F+1)-th subband becomes possible and the conductance $G(V)$ undergoes a positive jump. Such jumps are repeated for increasing voltage for all higher subbands. For $eV < 0$, when electrons tunnel from the thin film into bulk metal (Fig. 3,*b*) the situation is somewhat different. If the bias $|eV|$ becomes larger than distance $\Delta\varepsilon$ between the bottom of the last partially filled subband $\varepsilon_N = \pi^2\hbar^2 N_F^2/2m^*d^2$ and Fermi energy, $\Delta\varepsilon = \varepsilon_F - \varepsilon_N$, the contribution of the N_F-th subband to the tunnel current does not depend on the voltage because for any $|eV| > \Delta\varepsilon$ all electrons of this subband can tunnel into the bulk states of the left conductor. For this reason the differential conductance drops for values of $|eV|$ coinciding with bottoms of subbands of size quantization in the film. The distance between neighboring jumps of the conductance on the voltage scale equals the distance between energy levels $\Delta\varepsilon_N = \varepsilon_{N+1} - \varepsilon_N = \pi^2\hbar^2(2N_F+1)/2m^*d^2$. For $eV < 0$ the number of conductance jumps is finite and equals the number of discrete levels below Fermi surface N_F. The asymmetry around $V = 0$ and the general shape of the jumps in the conductance can be recognized in the experiments, see, e.g., [15]. In the special case of a 2D electron system, which has only one level in the potential well, there is a single negative jump of $G(V)$. Such a jump has been observed in Ref. 29 by STM investigations of the 2D electron gas at noble-metal surfaces. For $eV > 0$ the number of conductance jumps formally is not restricted. However, for $eV > \varepsilon_F$ our approach is no longer applicable and the influence of field emission on the tunnel current must be taken into account [30,31].

The observation of manifestations of the size quantization in the STM conductance requires a few conditions which must be fulfilled: The distance between the energy levels must be large enough and should satisfy the condition $\Delta\varepsilon_N \gg \hbar/\tau, T$, where τ is the mean scattering time of the electrons in the film and T is the temperature. The surfaces of the metal film in the region of the contact must be atomically smooth [32]. When a finite lifetime of the quantized states becomes relevant, the temperature broadening of the Fermi function, or surface imperfections need to be taken into account this will result in a rounding of the jumps in the curve $G(V)$ presented in Fig. 5 (Eqs. (20), (21)), which was plotted under assumptions of

perfectly specular surfaces, $T = 0$, and $\tau \to \infty$. With these restrictions taken into account the current–voltage curves in Fig. 4 give a fair qualitative description of the experimental results of Ref. 14.

It can be easily seen that the results obtained have a more wide domain of applicability than that of a rectangular well for the conducting film. For any model of the potential which restricts the electron motion in one direction the differential conductance has a step-like dependence on the applied bias with distances between the steps equal to the distances between the quantum levels.

5. Conclusion

In summary, we have investigated the conductance of ultra small contacts, for which the radius is smaller than the Fermi wave length, on top of the surface of a thin film. The discreteness of the component of the electron momentum transverse to the film surface is taken into account, where the distance between the electron energy levels due to the size quantization is assumed to be larger than the temperature. Both, a contact with a potential barrier of low transparency, and a contact without barrier have been considered. In framework of our model, using a δ-function potential barrier, the current–voltage characteristic $I(V)$ of the system and differential conductance $G(V)$ have been obtained. We predict a sawtooth dependence of $G(V)$ on the applied bias and show that the distance between neighboring jumps is equal to the distance between neighboring energy levels of size quantization, i.e., this dependence can be used for spectroscopy of size quantized levels. At $eV > 0$ the jumps in the conductance are positive and correspond to distances between levels above the Fermi surface, while $G(V)$ undergoes negative jumps for $eV < 0$, the distances between which are equal to the distances between the levels below the Fermi surface. The predicted quantization of the conductance can be observed in STS experiments, and the shape of the theoretical curves agrees well with experiments.

Appendix 1: Electron tunneling between the tip and the thin film

We search a solution to Eq. (1) at $V = 0$ in the form of a sum $\psi = \psi_0 + \psi_1$ for the incident and backscattered waves, and $\psi = \psi_1$ for the transmitted wave. Here ψ_0, as given by Eqs. (6), (8), is the unperturbed wave function that does not depend on the barrier amplitude U_0, while $\psi_1 \sim 1/U_0$ gives the first order correction. Substituting the wave function into the boundary conditions (2) and (3) one should match terms of the same order in $1/U_0$. As a result the boundary condition (3) becomes [7]

$$\psi_1(\boldsymbol{\rho}, 0) = -\frac{i\mathbb{k}\hbar^2}{m^* U_0} e^{i\boldsymbol{\kappa}\boldsymbol{\rho}} \Theta(a - \rho), \qquad \text{(A1.1)}$$

where $\mathbb{k} = k_z$ when the wave is incident to the contact from the tip side, and $\mathbb{k} = k_{zn}$ when the wave arrives at the contact from the sheet. For $ka \ll 1$ we have in the plane of the contact $\kappa\rho \ll 1$ and we can neglect the exponent in the boundary condition (A1.1).

The function $\psi_1(\boldsymbol{\rho}, z)$ can be represented as a Fourier integral

$$\psi_1(\boldsymbol{\rho}, z) = \int_{-\infty}^{\infty} d\boldsymbol{\kappa}' e^{-i\boldsymbol{\kappa}'\boldsymbol{\rho}} \Psi(\boldsymbol{\kappa}', z). \qquad \text{(A1.2)}$$

The Fourier components in (A1.2) should satisfy the zero boundary condition at $z = d$, but are otherwise freely propagating along z,

$$\Psi(\boldsymbol{\kappa}', z) = \Psi(\boldsymbol{\kappa}', 0) \frac{\sin k_z' (z - d)}{\sin k_z' d}, \quad 0 \leqslant z \leqslant d, \qquad \text{(A1.3)}$$

$$\Psi(\boldsymbol{\kappa}', z) = \Psi(\boldsymbol{\kappa}', 0) \exp(-ik_z' z), \quad z \leqslant 0, \qquad \text{(A1.4)}$$

with $k_z' = \sqrt{k^2 - \kappa'^2}$, $k = \sqrt{2m^*\varepsilon}/\hbar$. From Eqs. (A1.1), (A1.2) it follows that

$$\Psi(\boldsymbol{\kappa}', 0) = \frac{1}{(2\pi)^2} \int_{-\infty}^{\infty} d\boldsymbol{\rho} e^{i\boldsymbol{\kappa}'\boldsymbol{\rho}} \psi(\boldsymbol{\rho}, 0) = -\frac{i\mathbb{k}\hbar^2 a}{2\pi m^* U_0} \frac{J_1(\kappa' a)}{\kappa'}. \qquad \text{(A1.5)}$$

Substituting this into Eq. (A1.2) we find the wave functions for the electrons transmitted through the contact as

$$\psi_1(\boldsymbol{\rho}, z) = \frac{i\mathbb{k}\hbar^2 a}{m^* U_0} \int_0^{\infty} d\kappa' J_0(\kappa'\rho) J_1(\kappa' a) \frac{\sin k_z'(d - z)}{\sin k_z' d}, \quad 0 < z \leqslant d, \qquad \text{(A1.6)}$$

$$\psi_1(\boldsymbol{\rho}, z) = \frac{i\mathbb{k}\hbar^2 a}{m^* U_0} \int_0^{\infty} d\kappa' J_0(\kappa'\rho) J_1(\kappa' a) \exp(-ik_z' z), \quad z < 0, \qquad \text{(A1.7)}$$

where $J_n(x)$ is the Bessel function of the first kind.

Appendix 2: Metallic point contact between STM tip and metal film

Here we consider a point contact without potential barrier in the plane of the interface. When the contact radius is small, $ka \ll 1$, we can use perturbation theory for the electron wave function in the limit $a \to 0$. In zeroth approximation the wave functions are given by Eqs. (6) and (8). The first order correction, $\psi_1(\boldsymbol{\rho}, 0)$, to the wave function in the plane of the contact can be found by the method proposed in [25]. For distances $r \ll \lambda$ from the contact we can neglect the second term in the Schrödinger equation (1) and it reduces to the Laplace equation. We express the wave function in coordinates of an oblate ellipsoid of revolution (σ, τ, φ), with $\sigma \geqslant 0$ and $-1 \leqslant \tau \leqslant 1$. As a consequence of the cylindrical symmetry of the problem the

wave function $\psi_1(\sigma,\tau)$ does not depend on φ. The interface corresponds to $\tau = 0$ and the plane of the orifice is at $\sigma = 0$. In these coordinates we obtain the equation

$$\frac{\partial}{\partial\sigma}\left[(1+\sigma^2)\frac{\partial\psi_1}{\partial\sigma}\right]+\frac{\partial}{\partial\tau}\left[(1-\tau^2)\frac{\partial\psi_1}{\partial\tau}\right]=0, \quad \text{(A2.1)}$$

with the boundary condition at the interface

$$\psi_1(\sigma>0,\tau=0)=0. \quad \text{(A2.2)}$$

The solution of the boundary problem (A2.1), (A2.2) is

$$\psi_1(\sigma,\tau)=\tau[c_1\sigma+c_2(1+\sigma\arctan\sigma)], \quad \text{(A2.3)}$$

where c_1 and c_2 are constants. For $\sigma = 0$ Eq. (A2.3) gives the function $\psi_1(\boldsymbol{\rho},z)$ in the plane of the contact $z = 0$, $\rho \leqslant a$

$$\psi_1(\boldsymbol{\rho},0)=c_2\sqrt{1-\frac{\rho^2}{a^2}}. \quad \text{(A2.4)}$$

As in Appendix 1, we express $\psi_1(\boldsymbol{\rho},z)$ as a Fourier integral and, using the Eq. (A2.4), we find for the Fourier components

$$\Psi(\boldsymbol{\kappa}',0)=\frac{1}{(2\pi)^2}\int\limits_{-\infty}^{\infty}d\boldsymbol{\rho}e^{i\boldsymbol{\kappa}'\boldsymbol{\rho}}\psi_1(\boldsymbol{\rho},0)=c_2a\frac{j_1(\kappa'a)}{\kappa'}, \quad \text{(A2.5)}$$

where $j_1(x)$ is the spherical Bessel function of the first kind. Substituting Eq. (A2.5) into Eq. (A1.2) and using Eqs. (A1.3), (A1.4) we obtain

$$\psi_1(\rho,z)=\frac{c_2a}{2\pi}\int\limits_0^{\infty}d\kappa' J_0(\kappa'\rho)j_1(\kappa'a)\frac{\sin k_z'\,(d-z)}{\sin k_z'\,d}, \quad 0<z\leqslant d, \quad \text{(A2.6)}$$

and

$$\psi_1(\rho,z)=\frac{c_2a}{2\pi}\int\limits_0^{\infty}d\kappa' J_0(\kappa'\rho)j_1(\kappa'a)e^{-ik_z'z}, \quad z<0. \quad \text{(A2.7)}$$

The constant c_2 must be found from the boundary condition (3) at $U_0 = 0$, which for this case takes the form

$$\frac{\partial\psi_1(\rho,+0)}{\partial z}-\frac{\partial\psi_1(\rho,-0)}{\partial z}-2i\mathbb{k}=0. \quad \text{(A2.8)}$$

The meaning of the symbol $\mathbb{k}$ is explained below Eq. (A1.1). Differentiating Eqs. (A2.6) and (A2.7) with respect to z and calculating the integrals in the limit of small a we find

$$\left.\frac{\partial\psi_1}{\partial z}\right|_{z=+0}\simeq\frac{c_2a}{2\pi}\left[-\frac{\pi}{2a^2}+i\frac{\pi^3a}{18d^3}N(N+1)(2N+1)\right], \quad \text{(A2.9)}$$

$$\left.\frac{\partial\psi_1}{\partial z}\right|_{z=-0}\simeq\frac{c_2a}{2\pi}\left(\frac{\pi}{2a^2}+i\frac{\pi k^3a}{9}\right), \quad \text{(A2.10)}$$

where $N = [kd/\pi]$ with $[x]$ the integer part of x. Substituting Eqs. (A2.9) and (A2.10) into (A2.8) in leading approximation in a, in which only first terms in brackets (proportional to $1/a^2$) should be taken into account, we find for the unknown constant

$$c_2\simeq 2i\mathbb{k}a. \quad \text{(A2.11)}$$

1. W.A. Hofer, A.S. Foster, and A.L. Shluger, *Rev. Mod. Phys.* **75**, 1287 (2003).
2. J.M. Blanco, F. Flores, and Rubén Pérez, *Progr. Surf. Sci.* **81**, 403 (2006).
3. J. Tersoff and D. Hamann, *Phys. Rev. Lett*. **50**, 1998 (1983); *Phys. Rev*. **B31**, 805 (1985).
4. J. Bardeen, *Phys. Rev. Lett*. **6**, 57 (1961).
5. K. Kobayashi, *Phys. Rev*. **B53**, 11091 (1996).
6. Ye.S. Avotina, Yu.A. Kolesnichenko, A.N. Omelyanchouk, A.F. Otte, and J.M. van Ruitenbeek, *Phys. Rev*. **B71**, 115430 (2005).
7. I.O. Kulik, Yu.N. Mitsai, and A.N. Omelyanchouk, *Zh. Eksp. Theor. Phys*. **66**, 1051 (1974).
8. Ye.S. Avotina, Yu.A. Kolesnichenko, A.F. Otte, and J.M. Ruitenbeek, *Phys. Rev*. **B74**, 085411 (2006).
9. Ye.S. Avotina, Yu.A. Kolesnichenko, S.B. Roobol, and J.M. Ruitenbeek, *Fiz. Nizk. Temp*. **34**, 268 (2008) [*Low Temp. Phys*. **34**, 207 (2008)].
10. Ye.S. Avotina, Yu.A. Kolesnichenko, A.F. Otte, and J.M. Ruitenbeek, *Phys. Rev*. **B75**, 125411 (2007).
11. N.V. Khotkevych, Yu.A. Kolesnichenko, and J.M. van Ruitenbeek, *Fiz. Nizk. Temp*. **37**, 64 (2011) [*Low Temp. Phys*. **37**, 53 (2011)].
12. Ye.S. Avotina, Yu.A. Kolesnichenko, and J.M. van Ruitenbeek, *Fiz. Nizk. Temp*. **36**, 1066 (2010) [*Low Temp. Phys*. **36**, 849 (2010)].
13. I.B. Altfeder, K.A. Matveev, and D.M. Chen, *Phys. Rev. Lett.* **78**, 2815 (1997).
14. I.B. Altfeder, D.M. Chen, and K.A. Matveev, *Phys. Rev. Lett*. **80**, 4895 (1998).
15. C.-S. Jiang, H.-B. Yu, X.-D. Wang, C.-K. Shih, and Ph. Ebert, *Phys. Rev*. **B64**, 235410 (2001).
16. W.B. Su, S.H. Chang, W.B. Jian, C.S. Chang, L.J. Chen, and Tien T. Tsong, *Rev. Lett.* **86**, 5116 (2001).
17. I.B. Altfeder, V. Narayanamurti, and D.M. Chen, *Phys. Rev. Lett*. **88**, 206801 (2002).
18. Hongbin Yu, C.-S. Jiang, Ph. Ebert, and C.-K. Shih, *Appl. Phys. Lett.* **81**, 2005 (2002).
19. W.B. Jian, W.B. Su, C.S. Chang, and T.T. Tsong, *Phys. Rev. Lett.* **90**, 196603 (2003).
20. V.A. Gasparov, *Fiz. Nizk. Temp*. **37**, 1073 (2011) [*Low Temp. Phys*. **37**, 856 (2011)].

21. L.C. Davis, R.C. Jaklevic, and John Lambe, *Phys. Rev*. **B12**, 798 (1975).
22. A.I. Khachaturov, *J. Exp. Theor. Phys*. **91**, 541 (2000).
23. V.N. Lutskii, D.N. Korneev, and M.I. Elinson, *JETP Lett*. **4**, 179 (1966).
24. I.O. Kulik, A.N. Omel'anchuk, and R.I. Shekhter, *Fiz. Nizk. Temp*. **3**, 1543 (1977) [*Sov. J. Low Temp. Phys*. **3**, 740 (1977)].
25. I.F. Itskovich and R.I. Shekhter, *Fiz. Nizk. Temp*. **11**, 373 (1985) [*Sov. J. Low Temp. Phys*. **11**, 202 (1985)].
26. G.A. Korn and T.M. Korn, *Mathematical Handbook*, New York, Dover (2000).
27. Ye.S. Avotina, Yu.A. Kolesnichenko, and J.M. Ruitenbeek, *J. Phys.: Condens. Matter* **20**, 115208 (2008).
28. C. Berthod and T. Giamarchi, *Phys. Rev*. **B84**, 155414 (2011).
29. L. Bürgi, N. Knorr, H. Brune, M.A. Schneider, and K. Kern, *Appl. Phys*. **A75**, 141 (2002).
30. O.Yu. Kolesnychenko, O.I. Shklyarevskii, and H. van Kempen, *Phys. Rev. Lett*. **83**, 2242 (1999).
31. C. Pauly, M. Grob, M. Pezzotta, M. Pratzer, and M. Morgenstern, *Phys. Rev*. **B81**, 125446 (2010).
32. B.A. Tavger and V.Ya. Demikhovski, *Sov. Phys. Usp.* **11**, 644 (1969).